Wet ice cloud particles at subfreezing temperatures?

Valery Melnikov

University of Oklahoma, CIMMS, Norman, OK. valery.melnikov@noaa.gov

1. Introduction

Differential reflectivity Z_{DR} and the copolar correlation coefficient ρ_{hv} in liquid precipitation are well understood (e.g., Bringi and Chandrasekar 2001). At S frequency band, typical Z_{DR} values in rain lay in an interval from 0 to 3 dB and ρ_{hv} are typically larger than 0.98. The latter value is often used in recognition of rain in radar echoes. In cloud areas with ice particles, Z_{DR} values vary in a large interval and can reach 10 dB (e.g. Melnikov et al. 2011). Values of Z_{DR} in clouds and snowstorms are typically positive that signifies horizontal alignment of non-spherical particles, but negative Z_{DR} values have also been observed. Negative Z_{DR} have been observed in thunderstorms generating strong electrical fields that align ice crystals vertically (e.g., Hendry et al. 1987, Metcalf 1995, Caylor and Chandrasekar 1996). Negative Z_{DR} are also observed as a result of strong differential attenuation. In this paper, cloud areas with positive Z_{DR} located above the melting layers are examined. The temperature profiles from rawinsondes suggest subfreezing temperatures in the areas.

Values of ρ_{hv} in ice clouds are typically lower than those in rain but remain higher than 0.94. In section 3, localized cloud areas with ρ_{hv} smaller than 0.92 are examined. To analyze relations between Z_{DR} and ρ_{hv} in such areas, results of calculations are discussed in the next section. Then these results are applied to radar data (section 3) and some controversial findings are revealed and discussed. To explain the findings, two approaches are examined: the first is based on considerations of dry ice scatterers and the second involves a hypothesis of wet ice particles. These two approaches are discussed further in section 4.

2. Z_{DR} and ρ_{hv} of ice cloud particles

Values of Z_{DR} and ρ_{hv} in ice clouds are mutually connected; they depend on the shapes of particles, their spatial orientations, and bulk ice density. Orientations of cloud particles are characterized with the mean alignment angle and a distribution of orientations relative to this mean. The mean alignment angle is usually a direction of a particle's symmetry axis. For raindrops, the mean orientation angle of the droplet's minor axis relative to vertical is called the canting angle. In calm air, the canting angle of raindrops is zero (e.g., Huang et al, 2008). The term "canting angle" is used herein as well for the mean alignment angle of the symmetry axis of ice cloud particles. Positive Z_{DR} in ice clouds signify that particles are not spherical and fall down with their largest dimension oriented horizontally in the mean. Under calm air conditions, ice particles exhibit glide-pitch motions and spiral oscillations called "flutter" (e.g., Prupacher and Klett, 1997, section 10). All alternations in particles' orientations are called flutter herein for brevity.

The air temperature, pressure, and humidity, along with ice nuclei in clouds, determine the variety of ice particles' shapes: from simple plates and columns to complex rosettes, dendrites, and aggregates. Some shapes of cloud particles are shown in Fig. 1 (Peterson et al. 1975).

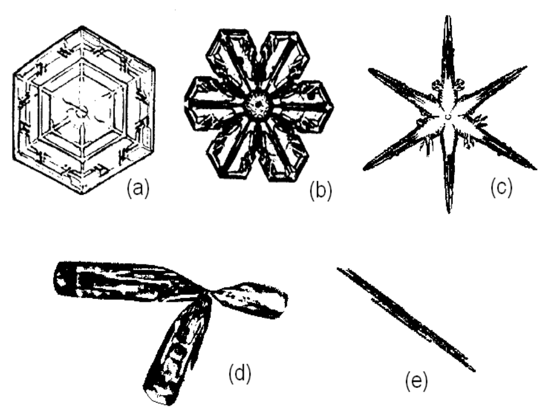

Fig. 1. Ice cloud particles in a form of: (a) a solid plate, (b) a sectored plate, (c) a dendrite, (d) a bullet, and (e) a needle (from Peterson et al. 1975).

To calculate scattering properties of ice cloud particles, various crystal shapes are often represented with spheroids that are close in shape. Particles in Figs 1a,b can be approximated with single oblate spheroids of different bulk ice densities. Particles in Figs. 1c,d can be represented with a few (or several) prolate spheroids representing the particle’s branches. A needle in Fig. 1e can be well approximated with a single prolate spheroid. Representations of particles with spheroids simplify scattering geometry significantly and allow obtaining useful relations between the particles’ shapes/dimensions and radar polarimetric parameters.

Values of Z_{DR} and ρ_{hv} for two basic shapes, i.e., plates (e.g., Fig. 1a) and columns (e.g., Fig. 1e), are considered herein; other shapes are briefly discussed in section 4. The geometry of scattering particles and incident radar waves are sketched in Fig. 2. Spheroids have two principal semi axes, *a* and *b* ($a \geq b$), and the axis of rotation, OO’. Orientation of a spheroid is characterized by two angles θ and φ between the axis of symmetry and the coordinate axes X, Y, and Z. The plane XOY is horizontal. The direction of propagation of electromagnetic waves is determined by vector $\boldsymbol{k}$ directed along the *x*-axis, i.e., horizontal incidence is considered, which is a good approximation for antenna elevations less than 7^{o}. The Cartesian coordinate system XYZ is natural for a cloud particle: its terminal fall velocity is directed along the Z-axis and angles θ and φ determine particle’s orientation uniquely. For plate-like particles, the mean canting angle θ is zero. Horizontally oriented columnar particles have the mean θ of 90^{o}. The width of distribution in θ is characterized with the standard deviation σ_{θ}.

In a polarimetric radar configuration with Simultaneously Transmitted And Received (STAR) of horizontally and vertically polarized waves, signal paths in the two radar channels are different so the transmitted and received waves acquire hardware phase shifts ψ_t and ψ_r. These phases are the system differential phases upon transmit and receive and their sum is the system differential phase $\psi_{sys} = \psi_t + \psi_r$.

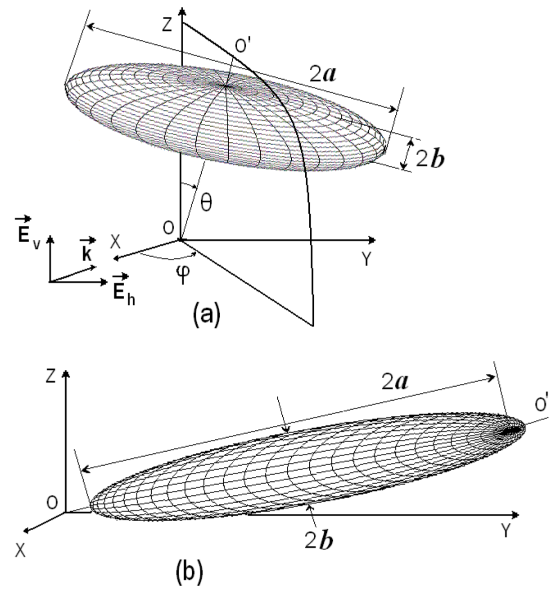

Fig. 2. Scattering geometry for (a) oblate and (b) prolate particles.

A cloud of nonspherical aligned scatterers shifts the phase between the horizontally and vertically polarized waves by the propagation differential phase φ_{dp} and differential phase upon scattering δ so that the measured phase shift is $\psi_{dp} = \psi_t + \psi_r + \varphi_{dp} + \delta = \psi_{sys} + \varphi_{dp} + \delta$. The phase δ upon scattering by ice cloud particles at cm-wavelengths is negligible. Thus propagation and scattering of polarized waves can be described for a STAR radar with the following matrix equation (e.g., Melnikov and Straka 2013):

$$\begin{pmatrix} E_{hr} \\ E_{vr} \end{pmatrix} = \mathrm{C} \begin{pmatrix} 1 & 0 \\ 0 & \exp[\, i(\psi_r + \frac{1}{2}\Phi_{dp})] \end{pmatrix} \begin{pmatrix} S_{hh} & S_{hv} \\ S_{hv} & S_{vv} \end{pmatrix} \times \begin{pmatrix} 1 & 0 \\ 0 & \exp[\, i(\psi_t + \frac{1}{2}\Phi_{dp})] \end{pmatrix} \begin{pmatrix} E_h \\ E_v \end{pmatrix}, \qquad (1)$$

where E_{hr} and E_{vr} are the received wave amplitudes, which are proportional to measured voltages in the polarization channels. The amplitude scattering matrix S_{ij} in (1) is bracketed by the matrices, which describe the propagation of the incident wave from the radar to the resolution volume and propagation of the scattered wave from the resolution volume back to the radar. C is a constant that depends on radar parameters and the range to the resolution volume.

The powers P_h , P_v in the receive channels and the correlation function R_{hv} of the signals are:

$$P_h = <|E_{hr}|^2>, \qquad P_v = <|E_{vr}|^2>, \qquad R_{hv} = <E_{hr}^* E_{vr}> , \tag{2}$$

where the brackets stand for ensemble averaging over particles' sizes and orientation angles; averaging is performed for particles in the radar resolution volume. Differential reflectivity Z_{DR} in dB and ρ_{hv} are

$$Z_{DR} = 10\log_{10}\frac{P_h}{P_v}, \quad \rho_{hv} = \frac{|R_{vh}|}{(P_h P_v)^{1/2}}. \tag{3}$$

Values of differential reflectivity in clouds are typically positive (in the absence of strong electric fields and differential attenuation) that means the particles fall down with their longest dimension being horizontal in the mean. Glide-pitch motions of cloud particles randomize the distribution on the horizontal plane, i.e., in angle φ. For the random φ-distribution, $<\sin\varphi> = <\sin^3\varphi> = 0$, $<\sin^2\varphi> = 1/2$, $<\sin^4\varphi> = 3/8$. The latter have been used in the calculations of Z_{DR} and ρ_{hv}. The distribution in θ is assumed to be the truncated Gaussian with standard deviation of σ_θ.

Eq. (1) has been used to obtain dependencies of Z_{DR} and ρ_{hv} upon the axis ratio *b/a* and for various σ_θ, where $\sigma_\theta = 90^o$ corresponds to the fully random distribution in θ. The dependences are shown in Fig. 3 for WSR-88D KOUN radar with $\psi_t = 82^o$. Z_{DR} and ρ_{hv} do not depend on ψ_r (Melnikov and Straka 2013). For the cases examined in the next section, the propagation differential phase can be neglected. Solid ice with density of 0.92 g cm^{-3} is assumed in the calculations. One can see that the maximal Z_{DR} are 10 dB and 4 dB for plates and columns respectively and are attained for very thin strictly horizontal particles. For completely random distributions in φ and θ, Z_{DR}= 0 dB regardless of *b/a*; so corresponding curves in Fig. 3(a) coincide with the horizontal axes. It is seen from Fig. 3(a) that if measured Z_{DR} exceeds 4 dB, it can be concluded that the particles have the plate-like shape.

The values of correlation coefficients of ice plates and columns are depicted in Fig. 3(b) for different σ_θ. At $b/a < 0.6$ and the same σ_θ, the difference in ρ_{hv} for plates and columns is considerable especially for weak flutter. For very thin nearly horizontal particles, ρ_{hv} is close to unity for plates and approaches 0.971 for columns which is due to random distribution in φ on the horizontal plane.

Fig. 3b can be used to estimate the maximum axis ratio *b/a*. For instance if $\rho_{hv} = 0.90$ (see cases in the next section), then we conclude from Fig. 3b that *b/a* is less than 0.22 regardless of the particles' shape (columns or plates) and values of σ_θ are quite high: columns must be oriented randomly and plates should have σ_θ larger than 40^o. Figs 3a,b can be used for estimations of particles axis ratios and σ_θ (Melnikov and Straka 2013).

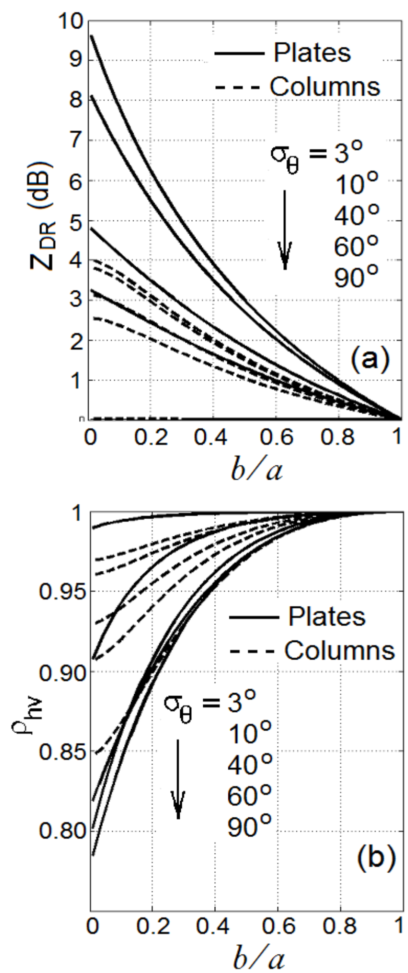

Fig. 3. (a) Z_{DR} and (b) ρ_{hv} for ice plates and columns as a function of the axis ratio b/a and various σ_θ for WSR-88D KOUN. Ice density of 0.92 g cm^{-3} has been used in the calculations.

3. Analysis of radar data

The data have been collected with the WSR-88D KOUN radar located in Norman, OK. The WSR-88D radars operate at a frequency band from 2700 to 3000 MHz and utilize the STAR polarimetric configuration. The operational WSR-88Ds collect data in a circular scanning regime (PPI) whereas the data from KOUN have been collected using true vertical cross sections (RHIs), i.e., the radar antenna was scanning in elevation at the same azimuth. This mode is very useful for detailed studies of clouds and precipitation. An example of RHI of a non-precipitating cloud is presented in Fig. 4 along with the rawinsonde data.

a. Case 2 March 2006.

The cloud within 60 km from the radar has reflectivity values lower than 25 dBZ (Fig. 4a) and exhibits moderate Z_{DR} with values lower than 2.5 dB (Fig. 4b). The values of correlation coefficient are higher than 0.95 (Fig. 4c). These are typical Z_{DR} and ρ_{hv} values for ice clouds. The cloud area beyond 60 km from the radar exhibits pockets of very high Z_{DR} (> 5 dB) having ρ_{hv} as low as 0.6. The correlation coefficients have been measured win KOUN with the lag-1 algorithm (Melnikov and Zrnic 2007), which is immune to noise impacts. So ρ_{hv} values in the area are not biased low by low signal-to-noise ratio. A distribution of Z_{DR} in this area is presented in Fig. 5a, where the frequency of occurrence is in the vertical axis. Corresponding mean values of ρ_{hv} as a function of Z_{DR} are depicted in Fig. 5b. One can see a positive slop in the mean ρ_{hv}: the values increase with increasing Z_{DR}. Such slopes are observed frequently in non-precipitating clouds (Melnikov and Straka 2013).

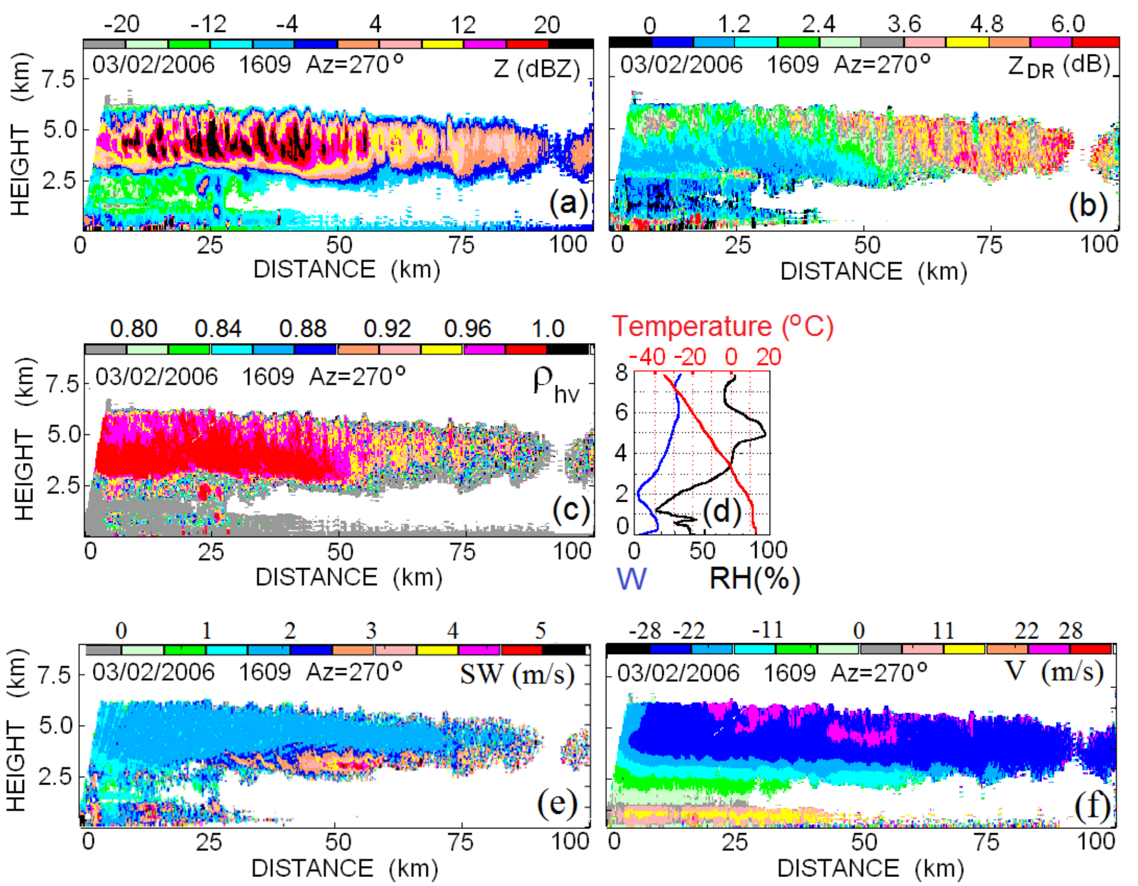

Fig. 4. Vertical cross sections of (a) reflectivity, (b) differential reflectivity, (c) the correlation coefficient, (e) spectrum width, (f) Doppler velocity collected with KOUN on March 2, 2006, at 1609Z at azimuth of 270^{o}. (d): Rawinsonde profiles of temperature (the red line), the wind speed (W in m s^{-1}, blue line), and relative humidity (RH, black line) obtained on the same day at Norman, OK at 1200Z.

Consider a part of the histogram in Fig. 5a in the proximity of Z_{DR} = 5 dB. Corresponding ρ_{hv} in Fig. 5b are of 0.90. A small area with ρ_{hv} of about 0.90 is shown in Fig. 6b with the blue rectangle. The curves in Fig. 6 are the same as in Fig. 3. One can see from Fig. 6b that the paticles must have the axis ratio *b/a* smaller than 0.22. Corresponding area with ZDR of about 5 dB and $b/a < 0.22$ is shown in Fig. 6a with the blue rectangle also. It follows from Fig. 6a that these particles must have the plate-like shape and σ_θ from 10^o to 40^o.

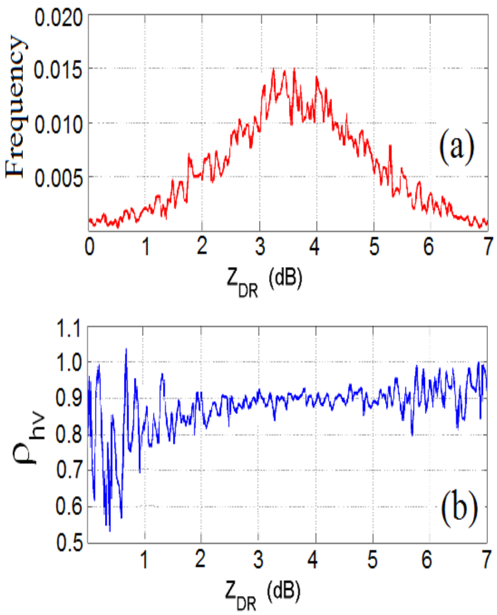

Fig. 5. (a): Frequency of occurrence of Z_{DR} values in cloud area beyond 60 km from the radar. RHI images are presented in Fig. 4. (b): The mean ρ_{hv} corresponding given Z_{DR}.

Next consider a part of the histogram in Fig. 5a close to Z_{DR} = 3 dB. Corresponding ρ_{hv} in Fig. 5b are of 0.90, for which we already deduced $b/a <$ 0.22. Corresponding area with Z_{DR} about 3 dB and $b/a < 0.22$ is shown in Fig. 6a with the green rectangle. It follows from Fig. 6b that for column-like particles, the σ_θ values must be larger than 60^o. From Fig. 6a we conclude that for such particles, σ_θ must be less than 40^o that contradicts the previous finding. Thus the particles cannot have column-like shape, they have to be plate-like. It follows from Fig. 6a that for plate-like particles, values of σ_θ must be in an interval $60^o > \sigma_\theta > 40^o$. Thus Z_{DR} of 3 dB and ρ_{hv} of 0.90 can be produced by plate-like particles with σ_θ within an interval 40 - 60^o. The latter is in contrast to $\sigma_\theta < 40^o$ obtained earlier for Z_{DR} about 5 dB.

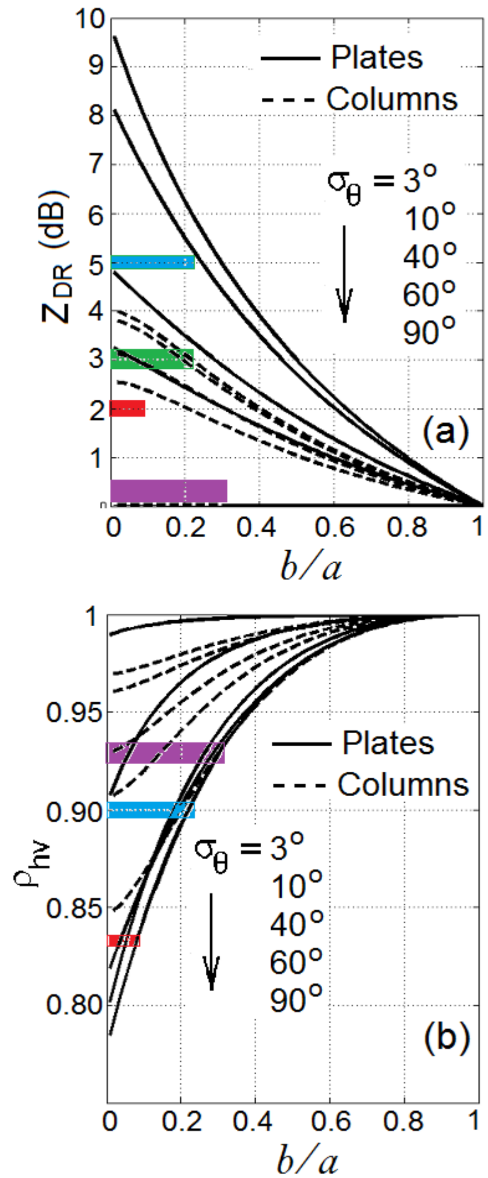

Fig. 6. Same as in Fig. 3. The colored rectangles are discussed in the text.

For Z_{DR} about 2 dB, the mean ρ_{hv} is about 0.83 (Fig. 5b). Corresponding area is shown in Fig. 6b with the red rectangle. This can only be produced by plate-like particles with $b/a < 0.1$. Corresponding area is shown in Fig. 6a with the red rectangle also. This rectangle lies in a region with $\sigma_\theta > 60^o$. Compare the conclusions drawn for particles having Z_{DR} of 5 and 2 dB belonging to the same cloud area. The particles with Z_{DR} = 5 dB have *b/a* < 0.22 and $\sigma_\theta < 40^o$. The particles with Z_{DR} = 2 dB have *b/a* < 0.1 and $\sigma_\theta > 60^o$. In both cases, the particles are very oblate because *b/a* are small, but more oblate particles have larger σ_θ, that is hard to explain. Intuitively, more oblate particles should be more stable in the air under the same ambient parameters. Particles with Z_{DR} of 5 and 2 dB belong to different radar volume, but these volumes are inside the same cloud area. Values of σ_θ are determined by particles' shape, sizes, ice density, and the intensity of small scale turbulence. To explain different σ_θ in the radar volumes, it seems necessary to accept variations in the turbulent intensity. Small scale turbulence is generated by larger scale turbulence, which is generated by the wind shear. No indications of strong wind shears in the areas are evident from the Doppler velocity and spectral width fields (Figs. 4e,f). There is a layer of wind shear located at a height of 3 km, i.e., below the area of low ρ_{hv}. So it is not clear how large and small σ_θ can coexist in radar volumes close to each other.

There could be other explanation of observed sufficiently large Z_{DR} and low ρ_{hv} in the area. Figs. 3 and 6 have been generated for dry ice particles. If ice particles have water on their surfaces, values of ρ_{hv} drop to ones observed in the melting layer. In this case under examination, the melting layer is located at heights from 2.6 to 2.8 km and can be seen in Fig. 4b. These heights correlate well with the freezing level from the rawinsonde temperature profile (Fig. 4d). The values of ρ_{hv} in the melting layer are the same as in the area under examination. The particles in the melting layer contain water in/on the ice particles that lower values of ρ_{hv}. The same cause could be responsible for lowering ρ_{hv} in the area under investigation. The temperatures in the area span an interval from -2^o to -10^oC. Reflectivity and differential reflectivity fields (Figs. 4a,b) exhibit vertically stretched patterns that could signify the presence of local updrafts. Such updrafts could carry warm air that could cause partial melting of small ice particles. The updrafts could also carry small water droplets, which could collide with ice particles and create a temporary water spots/films on particles' surfaces that could decrease ρ_{hv}.

b. Case 26 June 2007.

The radar vertical cross sections for this case are shown in Fig. 7. There are three areas of interest located between heights of 7.5 and 10 km at distances around 5, 60, and 75 km from the radar (Fig. 7c). Values of ρ_{hv} in the areas are lower than those in surrounding cloud areas. A distribution of ZDR values in the area at a distance around 75 km and 7.5 of height is depicted in Fig. 8a. One can see that Z_{DR} values are small in the area. Corresponding mean ρ_{hv} are shown in Fig. 8b. For Z_{DR} in an interval from 0 to 0.5 dB, the mean values of ρ_{hv} are about 0.92 -0.93. From Fig. 6b we obtain corresponding interval of *b/a*: *b/a* < 0.3. This area is shown in Fig. 6b with the magenta rectangle. Corresponding area with *b/a* < 0.3 and ZDR < 0.5 dB is shown in Fig. 6a with the magenta rectangle also. This area is located in a region with almost randomly distributed particles, i.e., with σ_θ close to 90^o. It is not clear why such oblate particles are oriented randomly and what mechanism is responsible for reshuffling the particles. Fields of the Doppler velocity and spectral width do not exhibit strong wind shears that could produce strong turbulence (Figs. 7e,f).

The temperatures in the area are from -10 to -25^oC (Fig. 7d). Values of ρ_{hv} in the area are the same as those in the melting layer located about 2 km below. The reflectivity field in a form of a bumped arc (Fig. 7a) allows speculating on the presence of updrafts above the melting layer. If so, these updrafts could be responsible for water on ice particles in the area and correspondingly low ρ_{hv} as it was discussed in the previous subsection.

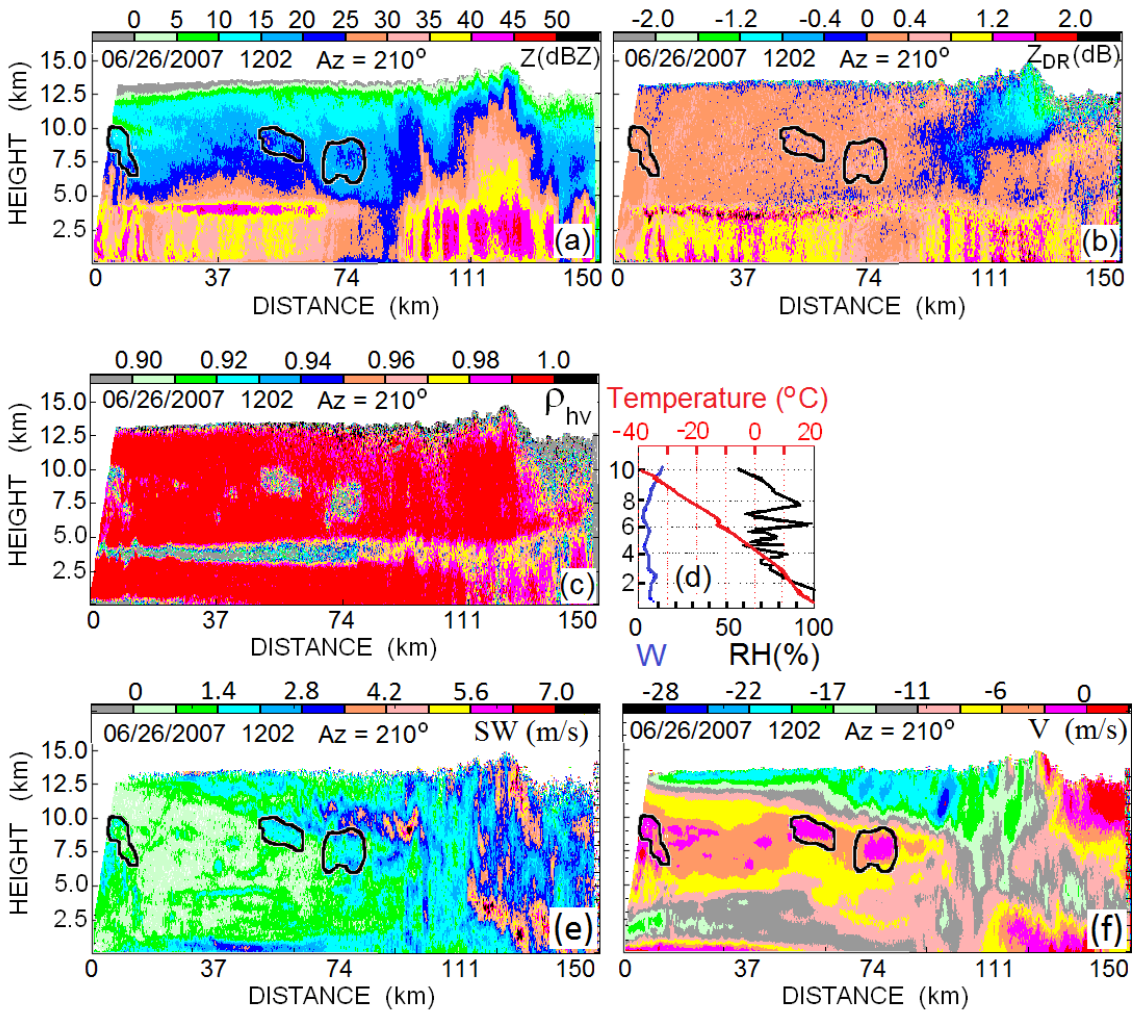

Fig. 7. Same as in Fig. 4 but for June 26, 2007 at 1202Z at azimuth of 210°. Rawinsonde profiles have been obtained on the same day at 1200Z at Lamont, OK. The black contours are the boundaries of the areas with low ρ_{hv} values in panel (c).

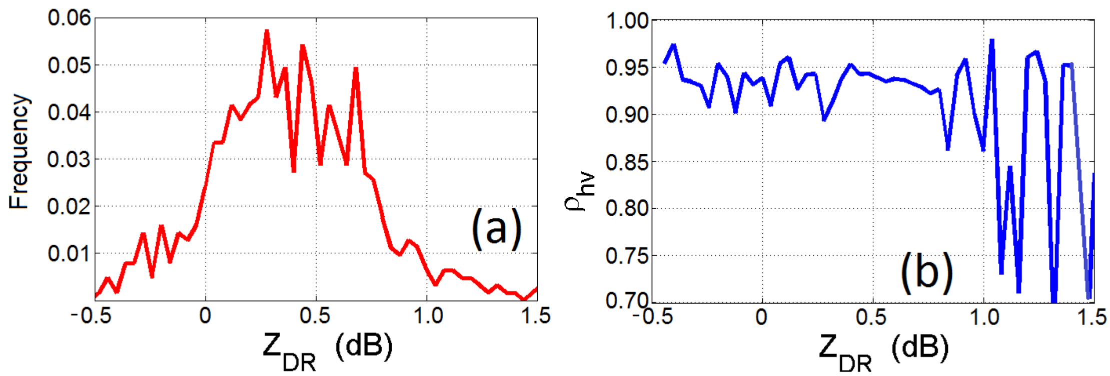

Fig. 8. Same as in Fig. 5 but for the area in Fig. 7c located around 74 km from the radar and at heights of about 7.5 km.

c. Case 14 July 2013.

The radar vertical cross sections for this case are shown in Fig. 9. One can see an area with low ρ_{hv} located between heights of 5.5 and 6.5 and distances between 13 and 25 km (Fig. 9c). The mean values of ρ_{hv} in the area are about 0.92 - 0.93, which are close to values observed in the melting layer. The temperatures in the area are from -7 to -12^{o}C (Fig. 9d). The area is located in a region with low spectral widths (panel e) and small velocity gradients (panel f); the outer boundaries of the area are shown with the black contour. Values of ρ_{hv} in the area are about 0.92 and can be caused by thin ice particles but this area is surrounded by cloud zones with lower Z_{DR} and it is hard to understand how the area with high Z_{DR} and low ρ_{hv} can develop inside cloud regions with typical Z_{DR} and ρ_{hv} values. The most striking observation is the equality of ρ_{hv} values in the area and in the melting layer located 1.5 km lower.

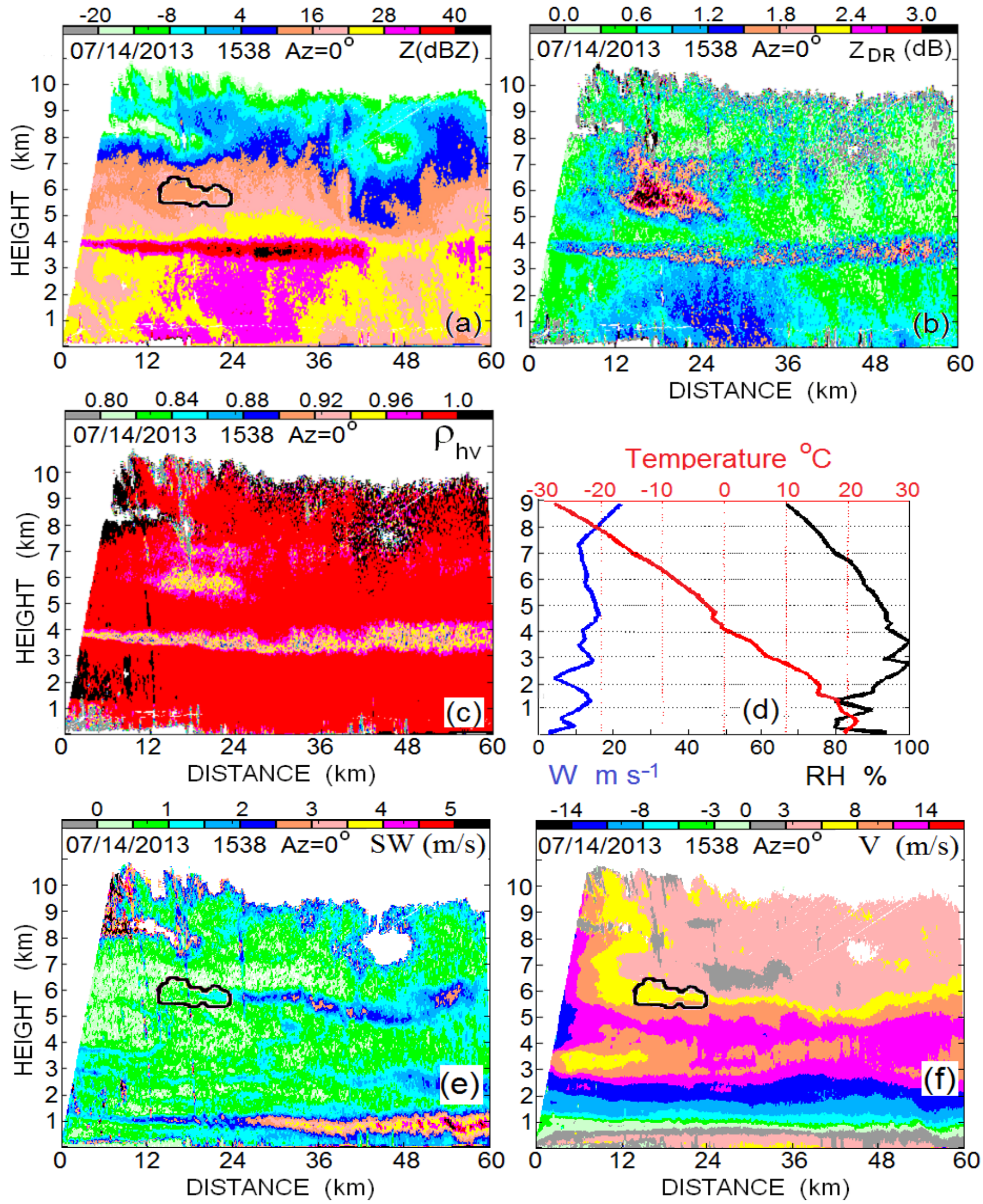

Fig. 9. Same as in Fig. 7 but for July 14, 2013 at 1538Z at azimuth of 0^{o}. Rawinsonde profiles have been obtained on the same day at KOUN at 1200Z.

4. Discussion

The cases examined in section 3 exhibit the presence of localized areas of low ρ_{hv} values surrounded by cloud regions with typical ρ_{hv} values in ice clouds. The areas lay at subfreezing temperatures. The values of ρ_{hv} in the areas are close to those observed in the melting layers. Ikeda et al. (2005) documented cases when radar observed two melting layers located at different heights. Those two melting layers correlated well with heights at which the temperature was 0^{o}C. The cases considered in the previous section are different: no temperature inversions are evident from the rawinsonde data. The rawinsonde's temperatures in the areas are substantially lower than 0^{o}C.

Low values of ρ_{hv} in the areas examined in section 3, could be caused by ice particles with large σ_{θ}. In case of 2 March 2006, such σ_{θ} should be quite variable in adjacent radar volumes. Values of σ_{θ} are determined by fluttering of particles in the air. Fluttering depends on particles' parameters (the sizes, shapes, ice densities) and also on the intensity of small-scale turbulence (e.g., Klett 1995). The particles in the examined areas are sufficiently oblate (*b/a* < 0.2) so that they should exhibit low to moderate σ_{θ} in still air. The large variations in σ_{θ} values should be due to variations in the intensity of small-scale turbulence. The latter depends on a larger scale turbulence, which is typically generated by the wind shears. No indications of significant wind shears in the areas are evident from the Doppler velocity and spectral width fields. So it is hard to explain the significant variations in σ_{θ} in adjacent radar volumes. Similar conclusions have been drawn for two other cases examined in the previous section.

Experimental results on σ_{θ} for ice crystals are sparse. Photogrammetric measurements of Kajikawa (1976) indicated canting angles of 10°–25°. Zikmunda and Vali (1972) found that 40% and 90% of rimed columnar crystals fell with less than 5° and 15^{o} canting correspondingly, but the canting was as large as 75° for a few crystals. Matrosov et al. (2005) found the intensity of flutter from 3^{o} to 15^{o} for three analyzed cases. The latter numbers correlate well with those obtained by Melnikov and Straka (2013). The available experimental data allow concluding that cloud ice particles typically experience weak to moderate flutter. The cases examined in section 3 exhibit large σ_{θ}. The areas with large σ_{θ} have been surrounded by regions of low σ_{θ}. It is not clear what mechanism is responsible for strong flutter in the areas with low ρ_{hv}.

The following are three assumptions made in generation of Fig. 3 that was used in the estimations of σ_{θ}.

1) The figure has been generated for two simple forms of particles: plates and columns whereas cloud particles' habits exhibit large variability (e.g., Fig. 1). Can ice particles of any shape produce lower ρ_{hv} than those for plates and needles? This seems unlikely. The majority of crystal habits can be represented with more simple shapes, i.e., plates and columns. It can be shown that composite particles have values of Z_{DR} and ρ_{hv} in between those for plates and columns. This also holds for 3-dimentional particles like the bullet in Fig. 1d. Most likely, arbitrary crystal habits cannot change the above conclusions drawn for plates and columns.

2) Fig 3 has been generated for solid ice with density of 0.92 g cm^{-3}. Cloud particles as in Fig. 1b,c are often represented with plates having bulk density lower than that for solid ice. Can lower bulk ice density change the above conclusions? No. Lower ice densities make Z_{DR} lower and ρ_{hv} higher than those for solid ice. This leads to a deduction of stronger flutter or to a conclusion that such a Z_{DR} - ρ_{hv} pair cannot belong to an ice particle.

3) Radar signal fluctuates in time so measured Z_{DR} and ρ_{hv} are estimates, which can deviate from the mean values. The intensity of signal fluctuations is strong at ρ_{hv} less than 0.90. The discussions in section 3 that involve Fig. 6 are based on the numbers that are close to the mean values of Z_{DR} and ρ_{hv} obtained from Figs. 5 and 8. Values of ρ_{hv} lower than 0.8 in Figs. 5 and 8 have not been considered because of strong fluctuations in the estimates. If the mean values are considered for such ρ_{hv}, interpretations of Z_{DR} - ρ_{hv} pairs using ice particles become more problematic because they require either exceptional flutter or cannot be explained at all.

Values of ρ_{hv} in the areas examined in section 3 are suspiciously close to the ones in the melting layers. Small water patches/films on the surface of ice particles can decrease ρ_{hv} to a level of 0.9 and lower so that no assumption on strong flutter of particles is needed. There is some indication of updrafts in reflectivity fields in Fig. 7 and 9: the reflectivity fields exhibit arc-like patterns in cloud regions beneath the areas with low ρ_{hv}. The updrafts could carry moisture and small droplets that could interact with small ice particles and create temporary water spots/films on the particles' surfaces (riming). If such patches/films exist on ice particles, the ρ_{hv} values can drop to levels of 0.9 – 0.8 like it occurs in the melting layers.

If the areas of low ρ_{hv} above the melting layers contain wet ice particles, such zones will be subject to aircraft icing. If an airplane flying at altitudes of a subfreezing temperature enters areas with wet ice particles, such particles will quickly convert to ice on the airplane's metal parts because of their high thermal conductivity. Thus areas of low ρ_{hv} above the melting layer could be dangerous for flights.

References

Bringi, V. N., and V. Chandrasekar, 2001: *Polarimetric Doppler Weather Radar. Principles and Applications.* Cambridge University Press. 636 pp.

Caylor I.J., and V. Chandrasekar, 1996: Time-varying ice crystal orientation in thunderstorms observed with multiparameter radar. *IEEE Trans.* **GRS-34**, 847-858

Ikeda, K., E. Brandes, R. M. Rasmussen, 2005: Polarimetric Radar Observation of Multiple Freezing Levels. *J. Atmos. Sci.*, **62**, 3624–3636.

Hendry, A., Y. Antar, and G. McCormick , 1987: On the relationship between the degree of preferred orientation in precipitation and dual-polarization radar echo characteristics. *Radio Sci.*, **22**, 37-50.

Huang G-J., V.N. Bringi, and M. Thurai, 2008: Orientation angle distributions of drops after an 80-m fall using a 2D video disdrometer. *J. Atmos. Oceanic Technol.*, **25**, 1717-1723.

Kajikawa, M., 1976: Observation of falling motion of columnar snow crystals. *J. Meteor. Soc. Japan,* **54,** 276–283.

Klett, J. D., 1995: Orientation Model for Particles in Turbulence. *J. Atmos. Sci.*, **52**, 2276–2285.

Matrosov, S. Y., R. F. Reinking, and I. V. Djalalova, 2005: Inferring fall attitudes of pristine dendritic crystals from polarimetric radar data. *J. Atmos. Sci.*, **62**, 241–250.

Melnikov, V.M., and D.S. Zrnic, 2007: Autocorrelation and cross-correlation estimators of polarimetric variables. *J.Atmos. Oceanic Technol*., **24**, 1337-1350.

Melnikov, V. M., D. S. Zrnić, R. J. Doviak, P. B. Chilson, D. B. Mechem, Y. Kogan, 2011: Prospects of the WSR-88D radar for cloud studies. *J. Appl. Meteor. Climatol.*, **50**, 859–872.

Melnikov, V., and J. Straka, 2013: Axis ratios and flutter angles of ice cloud particles: Retrievals from radar data. *J. Atmos. Oceanic Technol.*, **30**, 1691-1703.

Metcalf, J.I., 1995: Radar observations of changing orientations of hydrometeors in thunderstorms. *J. Applied Meteorol.*, **34**, 757-772.
.

Peterson, T.C., J-D. Yen, and W.R. Cotton. 1975: Manual for Snowflake observations, Identification, and Replication. Colorado State University. 31 pp.

Pruppacher, H. R., and J. D. Klett, 1997: *Microphysics of Clouds and Precipitation*. Kluwer Academic, 954 pp.

Zikmunda, J., and G. Vali, 1972: Fall patterns and fall velocities of rimed ice crystals. *J. Atmos. Sci.,* **29,** 1334–1347.